Boundary-Layer Meteorology (2019) 171:151–173
https://doi.org/10.1007/s10546-019-00426-7

RESEARCH ARTICLE

Interaction of Submeso Motions in the Antarctic Stable Boundary Layer

Daniela Cava[1] · Luca Mortarini[2,4] · Domenico Anfossi[4] · Umberto Giostra[3]

Received: 18 April 2018 / Accepted: 2 January 2019 / Published online: 18 January 2019

Abstract
Submeso motions add complexities to the structure of the stable boundary layer. Such motions include horizontal meandering and gravity waves, in particular when the large-scale flow is weak. The coexistence and interaction of such submeso motions is investigated through the analysis of data collected in Antarctica, in persistent conditions of strong atmospheric stratification. Detected horizontal meandering is frequently associated with temperature oscillations characterized by similar time scales (30 min) at all levels (2, 4.5 and 10 m). In contrast, dirty gravity waves superimposed on horizontal meandering are detected only at the highest level, characterized by time scales of a few minutes. The meandering produces an energy peak in the low-frequency spectral range, well fitted by a spectral model previously proposed for low wind speeds. The coexistence of horizontal and vertical oscillations is observed in the presence of large wind-direction shifts superimposed on the gradual flow meandering. Such shifts are often related to the variation of the mean flow dynamics, but also to intermittent events, localized in time, which do not produce a variation in the mean wind direction and that are associated with sharp decreases in wind speed and temperature. The noisy gravity waves coexisting with horizontal meandering persist only for a few cycles and produce bursts of turbulent mixing close to the ground, affecting the exchange processes between the surface and the stable boundary layer. The results confirm the importance of sharp wind-direction changes at low wind speed in the stable atmosphere and suggest a possible correlation between observed gravity waves and dynamical instabilities modulated by horizontal meandering.

Keywords Gravity waves · Horizontal meandering · Intermittent turbulence · Stable boundary layer · Wind-direction variability

✉ Daniela Cava
d.cava@isac.cnr.it

1 Institute of Atmospheric Sciences and Climate - National Research Council, Lecce, Italy

2 Universidade Federal de Santa Maria, Santa Maria, Brazil

3 Department of Pure and Applied Sciences (DiSPeA), Università degli Studi di Urbino "Carlo Bo", Scientific Campus "E. Mattei", 61029 Urbino, Italy

4 Institute of Atmospheric Sciences and Climate - National Research Council, Turin, Italy

1 Introduction

The stable boundary layer (SBL) is determined by a complex mix of anisotropic and intermittent turbulence and larger-scale processes that mainly includes non-stationary submeso motions (Mahrt 2014). Even if progress has been made in understanding various aspects of the SBL (for a review, see Sun et al. 2015a), the characteristics of interactions between turbulence and submeso motions are yet poorly understood, but they represent a critical problem for a correct estimation of the land-surface exchange and for improving numerical model performance in stable conditions (Mahrt 2014; Nappo et al. 2014). The interaction between such processes greatly influences turbulent energy and turbulent fluxes that are often weak, intermittent and difficult to correctly parametrize (Sun et al. 2015a). As a consequence, numerical models have difficulties in simulating the SBL, particularly in strongly stable conditions. As a matter of fact, the behaviour of turbulent and non-turbulent motions in the SBL is not well described by the classical theories of the atmospheric boundary layer (ABL) and this lack of understanding increases with increasingly stable stratification (Belušic and Güttler 2010; Güttler and Belušic 2012; Acevedo et al. 2014).

Submeso motions generally refer to any non-turbulent motions smaller than those traditionally classified as mesoscale. They include a complex mix of non-stationary and stochastic processes of different natures (such as density currents, microfronts, gravity waves, and horizontal meandering) on scales that separate the main turbulent eddies (in stable conditions these may be restricted to a few metres) and the smallest mesoscale motions (≈ 2 km) (Mahrt 2014; Sun et al. 2015a). Even if submeso motions exist under all atmospheric stratifications with weak large-scale flow (Anfossi et al. 2005), they have a crucial influence on boundary-layer structure under strong stratification because in these conditions turbulence production is closely related to local short-term accelerations associated with submeso motions even at large Richardson numbers (Mahrt 2011a; Mahrt et al. 2012).

Wave-like motions in the atmosphere are a common phenomenon and are also a fundamental feature of the SBL (Nappo 2002). Among them gravity waves and horizontal meandering require particular attention for their possible interaction and their role in intermittent turbulent production in very stable conditions.

Gravity waves observed in the SBL are rarely linear and clean oscillations characterized by constant amplitude and period. Instead, they are often solitary waves or occur in local packets and consist of only a few cycles with changing amplitude and period. These non-stationary and unstable 'dirty' waves frequently degrade and lead to a localized generation of turbulence enhancing the intermittent character of turbulent transport of momentum, mass and energy in very stable conditions (Nappo et al. 2014). Dirty waves cannot be easily parametrized and hence they are not accounted for in numerical models. Further, the wave–wave interaction and the interaction with turbulence may also be complicated by the possible interaction with other types of submeso motions such as, for example, horizontal meandering.

Horizontal-meandering modes represent an important fraction of submeso motions mainly observed near the surface in low-wind-speed and stable conditions. There is not a general consensus on the physical causes responsible for horizontal meandering, which can include pulsating drainage flows, surface pressure perturbations induced by mesoscale motions, and internal gravity waves (Mahrt 2007).

Meandering generally refers to large oscillations of the horizontal velocity components, often also associated with temperature oscillations (Mortarini et al. 2016a). Horizontal meandering has a strong influence on the dispersion of pollutants, in particular for its role in horizontal transport in the presence of weak vertical turbulent mixing (Mahrt and Mills 2009).

Since dispersion models generally underestimate meandering, they tend to overestimate pollutant concentrations (Anfossi et al. 2006; Belušic and Güttler 2010). Moreover, although meandering is normally associated with smooth oscillations in wind direction, sudden and sharp wind-direction shifts are often superimposed (Mahrt 2008). Such sudden shifts may produce strong directional shear associated with significant mixing events and represent a serious problem for simulating nocturnal dispersion because their causes are unknown (Lang et al. 2018).

Gravity waves and horizontal meandering often coexist and may interact in the very stable boundary layer. Cava et al. (2017) analyzed a low-wind-speed stably-stratified night characterized by the coexistence of linear gravity waves and horizontal meandering with similar time scales, indicating the same triggering mechanism, i.e. the pressure perturbations. Both submeso motions contributed to an increase in turbulent energy, especially in the vertical velocity component. Mortarini et al. (2018) presented a complex analysis of a night-time period where the development of a nocturnal low-level jet triggered both horizontal meandering and gravity waves, and strongly influenced the turbulent mixing producing a layered structure of the SBL. Both these studies confirmed the important role of submeso structures in the production of intermittent turbulence during low-wind-speed regimes and very stable conditions.

The aim of the present study is to investigate the coexistence and interaction of horizontal meandering and gravity waves, rarely explored previously. Data collected above an Antarctic ice sheet during an austral summer are analyzed in order to investigate the interactions between different submeso motions and their influence on the turbulence field in stable conditions. Antarctica represents an ideal site because of the persistent and strong stratification of the ABL. To detect and characterize submeso motions different methodologies are combined: a detection technique based on the evaluation of Eulerian autocorrelation functions, specifically implemented for identifying submeso motions (Anfossi et al. 2005; Mortarini et al. 2016a, b); and the wavelet analysis applied for studying the nature of submeso motions, their temporal evolution and their contribution in the production of intermittent turbulence (Cava et al. 2017; Mortarini et al. 2018).

2 Experimental Set-Up

The analyzed dataset refers to a summer experimental campaign (from November 1993 to February 1994) performed on the Nansen ice sheet in Terra Nova Bay, Victoria Land, Antarctica (Fig. 1). The Nansen ice sheet is a permanently frozen branch of the Ross Sea, which penetrates for 50 km into a region surrounded by complex topography. The site is prevalently influenced by flow along the valley axis and by persistent conditions of stable thermal stratification. The micrometeorological tower was located at 74°41′58″S, 163°30′50″E, in the middle of a flat snowy homogeneous area (the star in Fig. 1). Wind velocity components (u, v, w) and sonic anemometer temperature (θ) were sampled at a frequency of 20.8 Hz at three levels (2, 4.5, and 10 m) above the surface by symmetric 3-axis ultrasonic anemometers (Gill Ins. Ltd.). Further details on the experimental campaign and the site characteristics can be found in Cava et al. (2005, 2015).

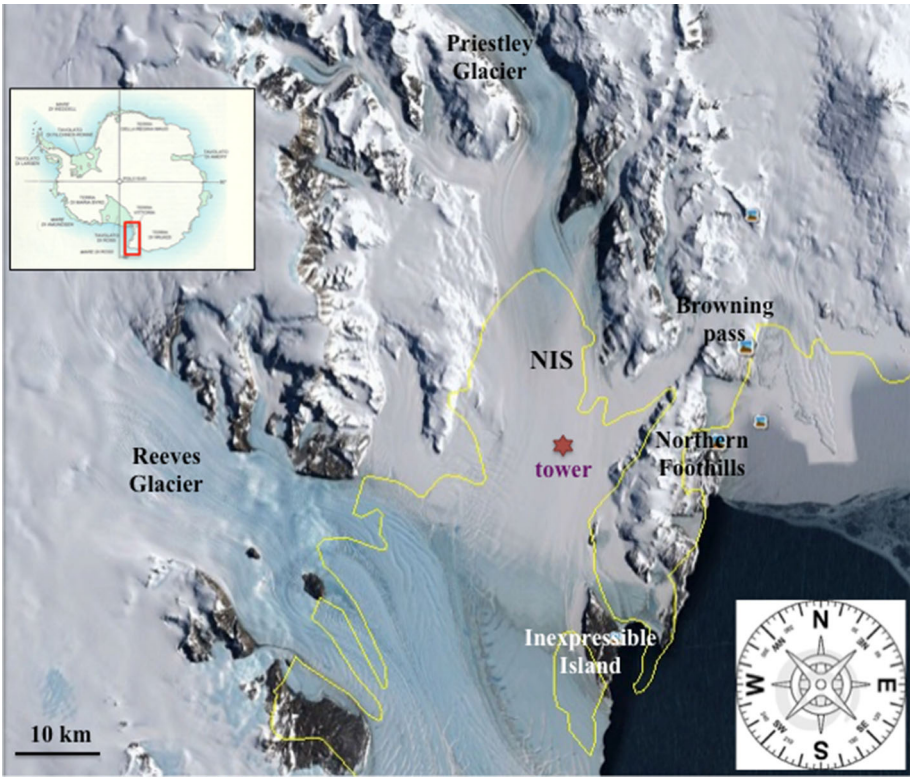

Fig. 1 Satellite image of Terra Nova Bay, Victoria Land (Antarctica). The star indicates the position of the micrometeorological tower located in the middle of a flat snowy homogeneous area on the Nansen ice sheet (NIS). The red rectangle in the inserted map indicates the position of Victoria Land in the Antarctic continent

3 Data Analysis

In order to investigate the coexistence and interaction of different submeso motions and their role in influencing the turbulent field in very stable conditions and in a flat and homogeneous area, data were analyzed using different techniques. The first step was to detect wavelike motions (Sect. 3.1) and then to study their spectral characteristics (Sect. 3.2); finally, the interaction of horizontal meandering, gravity waves and intermittent turbulence was investigated through wavelet analysis of selected case studies (Sect. 3.3). Before applying the Eulerian-autocorrelation-function detection technique and the spectral and wavelet analyses, the velocity components were rotated into the local streamline reference system by applying a triple rotation for each 60-min time series. Moreover, linear detrending of the data was applied only for the purpose of applying the Eulerian autocorrelation functions and the wavelet and Fourier analyses, in order to remove non-stationarity due to synoptic-scale variations that may produce red noise in the low-frequency spectral range, altering the detection of investigated submeso motions.

Finally, following Vickers and Mahrt (2006), for the filtering out of submeso contributions turbulent statistics were evaluated on 5 min subsets and then averaged over 1 h.

3.1 Detection of Submeso Motions

Submeso oscillations were detected in the hourly time series by applying a methodology proposed by Anfossi et al. (2005), based on the evaluation of the Eulerian autocorrelation functions of the main flow variables. In low-wind-speed and stable conditions the Eulerian autocorrelation functions frequently present an oscillatory behaviour that can be described by

$$R_x(\tau) = x(t+\tau)x(t)/\sigma_x^2 = \exp(-p_x\tau)\cos(q_x\tau) \quad \text{for} \quad x = u, v, w, \theta, \tag{1}$$

where σ_x^2 is the variance of the variable x, the parameter p is related to the turbulence decorrelation time scale, while the parameter q defines the meandering time scale

$$T_* = 2\pi/q. \tag{2}$$

The ratio between the q and p parameters defines the looping parameter $m = q/p$, which is crucial for meandering detection. Low values of m represent the absence of flow meandering, while high values of m (>1) indicate significant oscillations due to the submeso motions. The Anfossi et al. (2005) technique consists in fitting the Eulerian autocorrelation functions evaluated from the hourly time series with Eq. 1. The fitting procedure is based on the non-linear least-squares function of the R software (R Core Team 2017; Bates and Chambers 1992) that determines the non-linear least-squares estimates of the parameters of a non-linear model. The non-linear least-squares function provides an estimate (first guess) of the p and q parameters together with their standard error. The algorithm depends on the choice of the starting estimates of the two parameters, p and q. During the analysis we estimate the p and q parameters by performing the fit with 30 different couples of starting estimates, and then choosing the one that minimizes the residual standard deviation.

The Eulerian-autocorrelation-function technique applied to the 3-month dataset detected meandering activity of the horizontal velocity components (i.e. $m_u > 1$ and $m_v > 1$) in about 40% of analyzed hourly time series at all measurement levels, mainly during nocturnal hours (between 1600 and 0600 local time). About 50% of the detected horizontal oscillations were associated with temperature oscillations (i.e. $m_u > 1$ and $m_v > 1$ and $m_\theta > 1$). A clear dependence of detected horizontal-meandering episodes on surface features was not observed and small differences in the percentage of occurrence were found in different sectors of flow provenance. This behaviour suggests that oscillations due to horizontal meandering may be triggered by various mechanisms on the Nansen ice sheet, i.e. by both orographic features and by a horizontal temperature gradient (in particular above the sea sectors). Figure 2 shows the distribution of the obtained meandering time scales (Eq. 2) for detected hours. Horizontal velocity components and temperature appeared to be characterized by similar T_* (with modes between 20 and 30 min) that remained almost constant at the different heights. This result confirms that meandering of horizontal velocity components is often associated with temperature oscillations, as observed by Mortarini et al. (2016a).

On the other hand, vertical oscillations were detected by the Eulerian-autocorrelation-function technique only at the highest level in about 3% of the hours characterized by horizontal meandering. The Eulerian-autocorrelation-function methodology was originally implemented for identifying horizontal meandering motions (Anfossi et al. 2005), usually persistent for many cycles in the time domain. Instead, as is frequently observed (e.g., Mahrt 2014), vertical oscillations in the boundary layer are often related to dirty waves that last only a few cycles with variable amplitude and period.

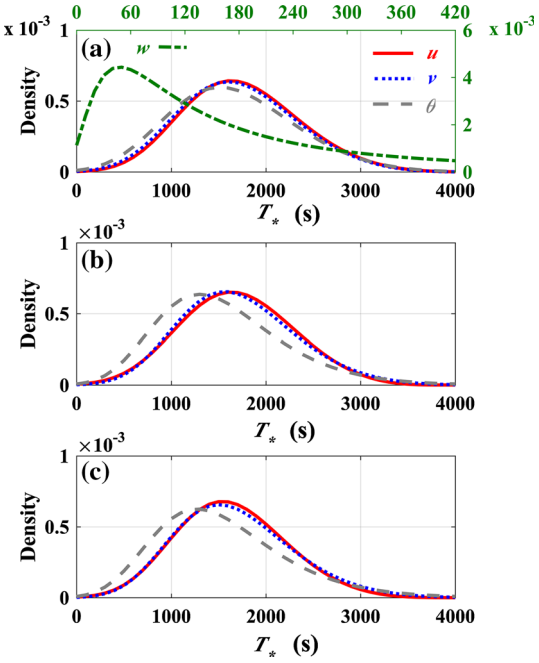

Fig. 2 Density distribution of meandering time scales for the analyzed variables collected at 10 m (**a**), 4.5 m (**b**) and 2 m (**c**). The distribution relative to the vertical velocity component shown only at the highest level (green curve) is associated with the top and right axes

Detected vertical waves were characterized by T_* of a few minutes (green dash–dotted curve in Fig. 2a, top and right axes) and smaller than those of coexisting horizontal velocity components and temperature oscillations. These short time scales agree with typical gravity-wave periods detected using other methods in the same dataset (Cava et al. 2015). Cava et al. (2015) also observed a degradation of vertical oscillations close to the ground. The observed disruption of gravity waves may be explained within the framework of the hockey-stick-transition (HOST) approach proposed by Sun et al. (2012), who classified the nocturnal turbulent mixing into weak and strong turbulent regimes depending on the relationship between wind speed and turbulence intensity (the square root of the turbulent kinetic energy ($\bar{e}$): $V_{\mathrm{TKE}} = \left(\left(\sigma_u^2 + \sigma_v^2 + \sigma_w^2\right)/2\right)^{1/2} = \bar{e}^{1/2}$). The weak regime corresponds to low wind speeds and turbulent eddies are generated by the local shear and do not directly interact with the ground. Turbulence intensity increases only slowly with increasing wind speed until it reaches a threshold value, and the strong turbulence regime prevails. In the strong regime, the turbulence is generated by the bulk shear and its intensity systematically increases with increasing wind speed. Because wind speed can readily exceed the corresponding threshold value near the ground, the influence of resulting turbulent mixing on gravity waves increases, producing less distinct vertical submeso oscillations at the lower levels (Sun et al. 2015b).

To verify the HOST transition in the analyzed dataset, the relationship between the wind speed (V) and the bin-averaged V_{TKE} at the three measurement levels in shown in Fig. 3. The arrow marks the transition between the weak and strong turbulence regimes at the highest measurement level. The observed wind-speed threshold (≈ 4.8 m s^{-1}) is similar to the value at 10-m height found by Sun et al. (2012). On the other hand, the transition between different turbulent regimes is less evident at the lowest heights because of the ground influence that increases the level of turbulent mixing contributing to the gravity-wave degradation close to the ground.

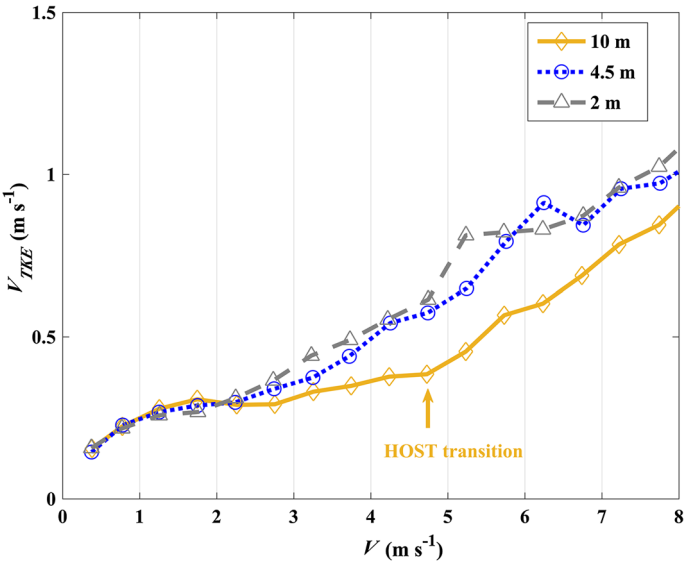

Fig. 3 Relationship between the wind speed (V) and the bin-averaged turbulence intensity ($V_{\mathrm{TKE}} = \bar{e}^{1/2}$) at the three measurement levels. The arrow marks the transition between the weak and strong turbulent regimes at the highest measurement level, similar to the hockey-stick transition (HOST) observed in Sun et al. (2012). This transition is less evident at the lowest levels because of the ground influence that increases the level of turbulence mixing

The density distribution of wind speed relative to the detected cases of horizontal meandering (Fig. 4) shows a peak of about 2.5 m s^{-1} at the highest level and coincident peaks of about 1.5 m s^{-1} at the lowest levels. The red arrow indicates the wind speed relative to the transition between the weak and strong turbulent regimes at the highest measurement level, as detected in Fig. 3. Even if the greatest percentage of horizontal-meandering cases occurs under a low-wind-speed regime, a non-negligible number of detected events are related to moderate wind speeds much higher than 2.5 m s^{-1}, in particular at 10 m.

3.2 Spectral Characteristics of Submeso Motions

In very stable conditions the coexistence of horizontal meandering, gravity waves and intermittent turbulence greatly alter the spectral shape of the main flow variables. Mortarini and Anfossi (2015) proposed an original relation for the spectra of velocity fluctuactions in low-wind-speed conditions and in the presence of horizontal meandering. Mortarini et al. (2016a) verified that such a relation could be applied to the air temperature too. The suggested approach takes into account the distribution of the flow energy in both turbulence and submeso scales and is able to describe in a unique function ($\tilde{F}$) both the low-wind-speed (F_{LW}) and the inertial subrange (F_{HW}) spectral behaviour,

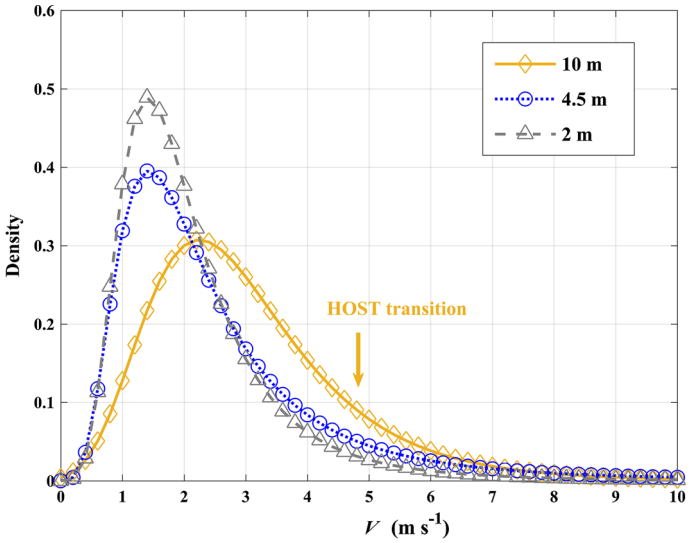

Fig. 4 Density distribution of wind speed referring to the horizontal meandering cases ($m_u > 1$ and $m_v > 1$) detected at the different measurement levels. The arrow indicates the wind speed relative to the transition between the weak and strong turbulent regimes at the highest measurement level, as detected in Fig. 3

$$\tilde{F}(\tilde{n}, m) = \frac{\alpha F_{LW}(\tilde{n}, p, q) + \beta(\tilde{n}) F_{HW}(\tilde{n})}{[n F_{LW}(n)]_{max}} \quad \tilde{n} = \alpha \frac{2\tilde{n}\left(1+\tilde{n}^2\right)}{m^2\left(1-\tilde{n}^2\right)^2 + \left(1+\tilde{n}^2\right)^2}$$
$$+ \frac{1 - 2\tilde{n} + \tilde{n}^2}{1 + 20\tilde{n} + \tilde{n}^2} \frac{0.515\frac{\tilde{n}}{\gamma}}{\sqrt{m^2+1}\left[1 + 0.0164\left(\frac{\tilde{n}}{\gamma}\right)^{5/3}\right]} \tag{3}$$

where n is the frequency in Hz, p, q and m are the parameters that describe the Eulerian-autocorrelation-function behaviour (Eq. 1), $\tilde{n} = n/n_{max}$ (with $n_{max} = \left(p^2+q^2\right)^{\frac{1}{2}}/(2\pi)$ representing the frequency relative to the F_{LW} maximum) and $\gamma = n_0/n_{max}$ (where n_0 is the frequency at which the extrapolated inertial subrange meets the $nF_{HW}(n) = 1$ line in the Kaimal and Finnigan (1994) (hereinafter, KF94) model for stable conditions). A detailed description of the low-wind spectral model is given in Appendix 1. It is worth noting that spectra lend themselves particularly well to an average over the whole dataset, since evaluating a mean of the Eulerian autocorrelation functions would be less straightforward.

Figure 5 shows the averaged normalized spectra of horizontal velocity components collected at the highest level (black continuous lines), relative to the meandering hours detected through the Eulerian-autocorrelation-function technique ($m_u > 1$ and $m_v > 1$). The spectra were computed from 1-h time series by using the fast Fourier transform technique. The spectra of both velocity components follow the Kolmogorov (1941) energy decay at inertial subrange scales (hereinafter, K41), but deviate from the typical turbulence spectrum at large scales, exhibiting a clear and energetic peak in the low-frequency range associated with horizontal-meandering oscillations. The spectra as a function of the normalized frequency $\tilde{n}$ have been compared with the low-wind-speed spectral model (Eq. 3) and then averaged over all the cases; the model (dotted lines) describes the spectral energy distribution well throughout the entire range of resolved frequencies.

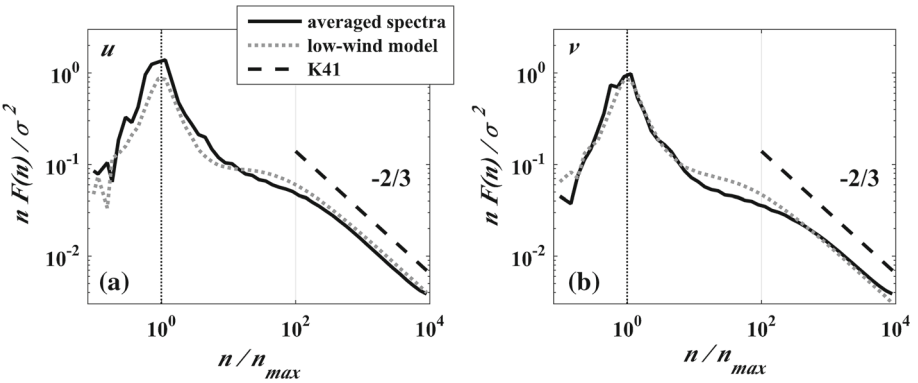

Fig. 5 Averaged normalized spectra (black continuous lines) of longitudinal (**a**) and lateral (**b**) velocity components collected at 10 m, referring to the meandering hours detected through the Eulerian autocorrelation function technique ($m_u > 1$ and $m_v > 1$). The grey dotted lines refer to the averaged low-wind-speed spectral model (Eq. 3), whereas the dashed lines refer to the K41 spectral law in the inertial subrange

As already specified in the previous section, about 50% of the detected horizontal oscillations are associated also with temperature oscillations (i.e. $m_u > 1$ and $m_v > 1$ and $m_\theta > 1$), whereas in only 3% of the meandering hours vertical oscillations are detected at the highest level (i.e. $m_u > 1$ and $m_v > 1$ and $m_w > 1$). Figure 6a, c displays the averaged spectra relative to the oscillating cases for the vertical velocity component and temperature, respectively. Both spectra exhibit a pattern similar to the horizontal velocity component spectra and appear well described by the low-wind-speed spectral model. The model was successfully applied to other temperature datasets (i.e. Mortarini et al. 2016a), but it is noteworthy that it also well reproduces the gravity-wave spectral shape for the investigated dataset, suggesting that the Eulerian-autocorrelation-function method can be applied to identify gravity-wave episodes in a large dataset, and their time scales compared with other submeso oscillations. Finally, Fig. 6b, d shows the averaged spectra relative to the w and θ non-oscillating cases during horizontal meandering (b: $m_u > 1$ and $m_v > 1$ and $m_w < 1$; and d: $m_u > 1$ and $m_v > 1$ and $m_\theta < 1$). They exhibit the typical shape of turbulence spectra and appear well fitted by the KF94 spectral model when plotted against the normalized frequency (n/n_0). This result confirms the good performance of the Eulerian-autocorrelation-function technique in detecting the oscillatory behaviour in all the flow variables and the robustness of the low-wind-speed spectral model.

3.3 Interactions of Submeso Motions and Wind-Direction Variability

The periods influenced by the coexistence of horizontal meandering and vertical waves detected by the Eulerian-autocorrelation-function technique were carefully analyzed to gain insight into the triggering and interaction mechanisms between different submeso motions. The visual analysis of the selected time series highlights the coexistence of horizontal meandering and gravity waves at the current experimental site, often associated with abrupt variations in the wind direction. In order to analyze and quantify the direction variability in the periods characterized by the occurrence of submeso motions, following Lang et al. (2018) the wind-direction changes have been computed as the difference between the subsequent 1-min wind direction and the previous 1-min wind direction, implying that the differences

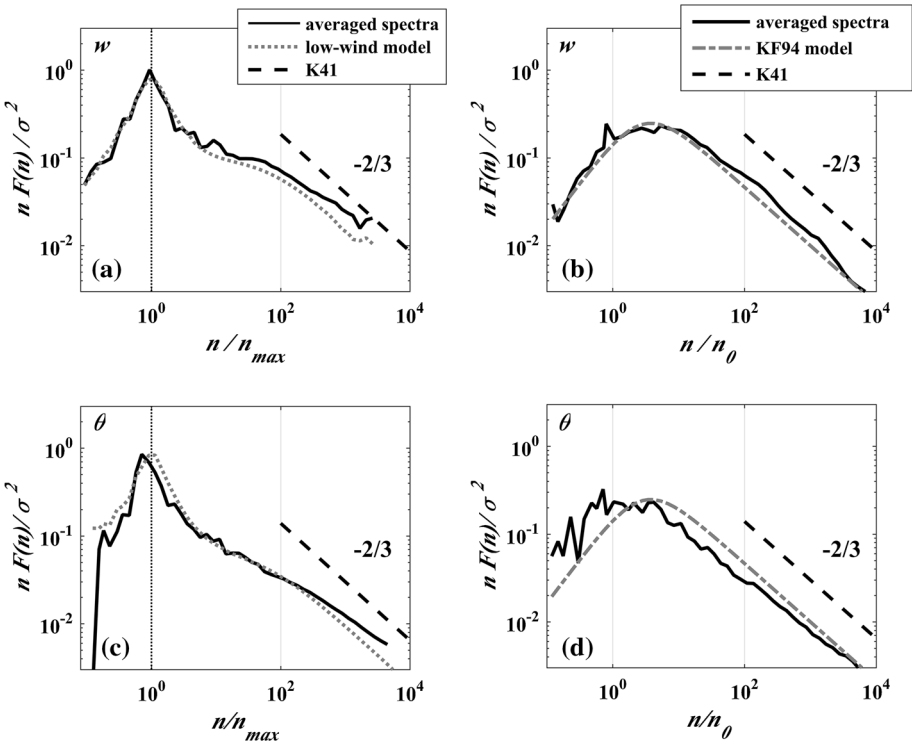

Fig. 6 Averaged normalized spectra (black continuous lines) of vertical velocity components (**a**, **b**) and temperature (**c**, **d**) collected at 10 m, referring to the meandering hours detected through the Eulerian autocorrelation function technique ($m_u > 1$ and $m_v > 1$). The left column refers to cases relative to detected low-frequency oscillations also in w ($m_u > 1$ and $m_v > 1$ and $m_w > 1$) and in θ (**c** $m_u > 1$ and $m_v > 1$ and $m_\theta > 1$) and the grey dotted lines refer to the average of the low-wind-speed spectral model (Eq. 3) evaluated for each case. The right column refers to cases where low-frequency oscillations in w (**b** $m_u > 1$ and $m_v > 1$ and $m_w < 1$) and in θ (**d** $m_u > 1$ and $m_v > 1$ and $m_\theta < 1$) are absent and the grey dashed-dotted lines refer to the averaged Kaimal and Finnigan (1994) spectral model (KF94) for stable conditions (Eq. A6). The dashed lines refer to the K41 spectral law in the inertial subrange

are centred across 2-min intervals. Moreover, computed wind-direction changes are reduced by 360° if they exceed 180°, or are increased by 360° if they are smaller than − 180°, such that they range between − 180° and 180°. Figure 7 shows the scatter plot of the 1-min wind-direction changes versus the 1-min wind speed for horizontal-meandering cases detected through the Eulerian-autocorrelation-function technique (black symbols: $m_u > 1$ and $m_v > 1$). The wind-direction changes appear inversely related to wind speed, consistent with Mahrt (2007, 2008, 2011b) and Lang et al. (2018) who investigated the influence of submeso motions on wind-direction variability and observed frequent abrupt shifts in wind direction with decreasing wind speed. The fraction of time that exhibits large and abrupt wind-direction shifts ($>\pm 20°$) is about 9% for each hour, and characterized by the occurrence of horizontal meandering. The obtained percentage remains unchanged for coexisting horizontal meandering and vertical low-frequency oscillations, but in these cases the largest wind-direction changes appear mainly associated with wind speeds lower than 2 m s^{-1} (red symbols: $m_u > 1$ and $m_v > 1$ and $m_w > 1$). Such a non-negligible percentage suggests

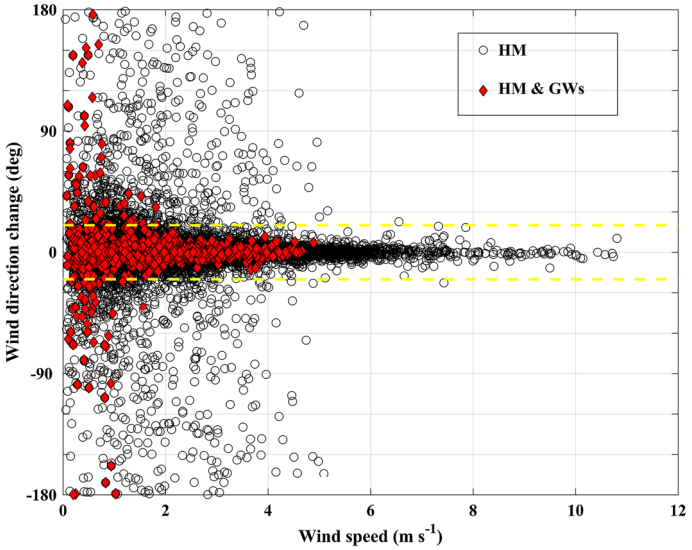

Fig. 7 Scatter plot of the changes of the 1-min wind direction versus the 1-min wind speed. Black empty circles are observations classified as horizontal meandering (HM) detected through the Eulerian autocorrelation function technique ($m_u > 1$ and $m_v > 1$), whereas red diamonds refer to cases relative to detected low-frequency oscillations also in w (GWs) ($m_u > 1$ and $m_v > 1$ and $m_w > 1$). The yellow horizontal dashed lines delimit the range of wind-direction change [$-20 \div 20$]

the importance of wind-direction variability in the flow dynamics of a low-wind-speed and stable atmosphere.

In the next sections two different nocturnal periods were selected as case studies representative of the observed interaction mechanisms between horizontal meandering, gravity waves and the turbulence field. The continuous wavelet analysis was applied to investigate the temporal evolution of the meandering time scales and to distinguish the interplay between horizontal meandering and vertical waves. The Morlet function was chosen as the mother wavelet for its high resolution in frequency space, suitable for a good estimation of the period of detected submeso motions (Thomas and Foken 2005). A brief description of wavelet analysis and cross-spectral gravity-wave indicators is given in Appendix 2.

3.3.1 Waves Associated with Sharp Variations in the Mean Flow Dynamics

The observed gravity waves coexisting with horizontal meandering in the analyzed dataset appeared frequently associated with sharp variations in the mean wind direction, often related with strong temperature falls and linked to sudden changes of airmasses and of the mean flow dynamics. As already observed previously (Viana et al. 2010; Sun et al. 2015b) such abrupt variations may generate uplifting as a result of the convergence between different airmasses, which may trigger dirty gravity waves that tend to degrade after a few cycles.

Figure 8 features an example of a nocturnal period characterized by the coexistence of horizontal meandering and dirty gravity waves. The night was characterized by low wind speeds (the mean wind speed ranged from 0.5 to 2.4 m s^{-1} at the highest level) and by the stability parameter $z/L \approx 1$, where z is the measurement height (10 m) and L is the Obukhov length. The time series of horizontal velocity components (Fig. 8a, b) exhibit a marked oscil-

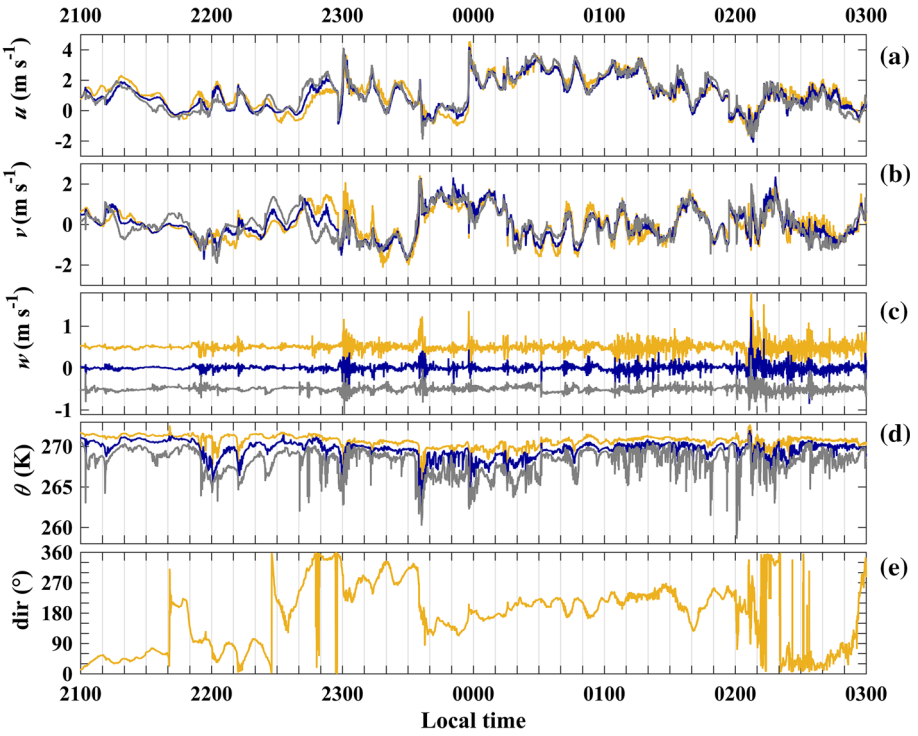

Fig. 8 Time series of longitudinal (**a**), lateral (**b**), vertical velocity components (**c**), temperature (**d**) and wind direction (**e**) collected at different measurement levels (yellow: 10 m, blue: 4.5 m, grey: 2 m) in the night between the 5 and 6 January 1994. For a better comparison the time series of w has been artificially shifted ($+0.5$ m s^{-1} at 10 m and -0.5 m s^{-1} at 2 m) in figure (**c**). Finally, for the sake of clarity the wind direction has been shown only at the highest level in panel (**e**)

latory behaviour from 2200 LT throughout all the analyzed period. The oscillatory behaviour is also evident in temperature (Fig. 8d) and in the wind direction (Fig. 8e). It is noteworthy that the gradual meandering in the wind direction appears recurrently interrupted by sudden mean wind-direction changes associated with large temperature falls and perturbations in the vertical velocity component (Fig. 8c). This is particularly evident at 2300, 2335 and 0210 LT.

The wavelet spectra provide an estimation of the time evolution of the signal energy at the different resolved time scales. Figure 9 shows the wavelet spectra for the analyzed signals collected at the highest level in the range of submeso time scales. The signature of horizontal meandering is highlighted by the increase in the wavelet energy density in the horizontal components, characterized by a time scale of about 10 min. The vertical component does not show any activity at the same time scale, but intermittently exhibits significant energy at smaller time scales at 2300, 2335 and 0210 LT, concurrently with the detected sharp wind-direction changes (see Fig. 8e). The maximum vertical energy is associated with a time scale of about 5 min, but propagates towards smaller scales, suggesting a perturbation of the turbulent field. The same analysis performed on the time series collected at the lower levels (not shown) displays the persistency of horizontal meandering at all measurement heights, but with attenuation of vertical wave energy closer to the ground. Finally, the distribution of temperature wavelet variance shows the signature of both horizontal and vertical flow

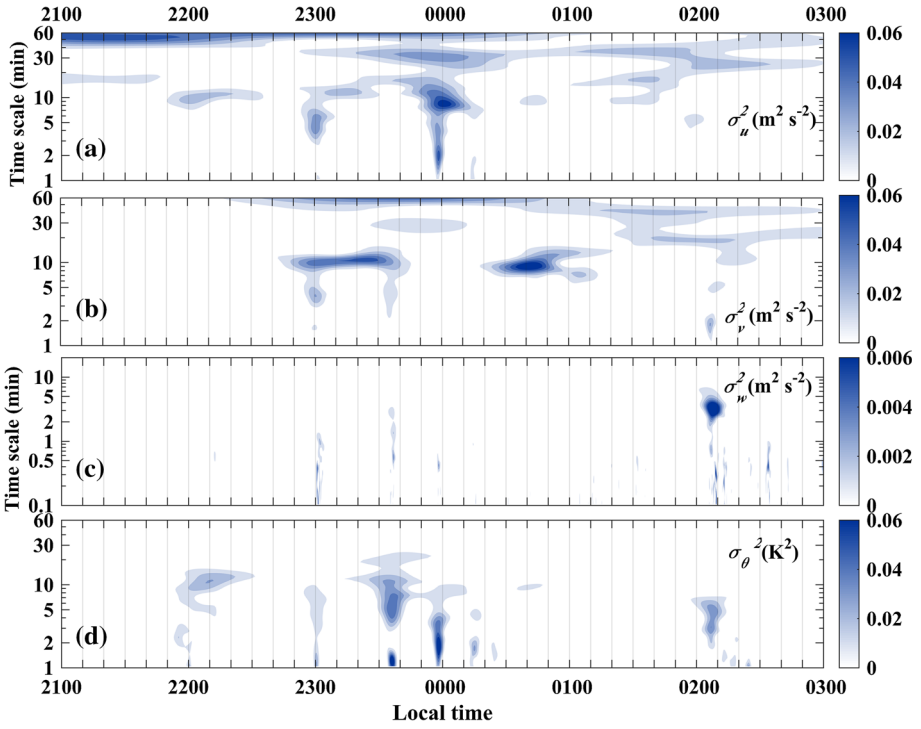

Fig. 9 Time evolution in the submeso time scale range of wavelet energy spectra of (**a**) longitudinal, (**b**) lateral and (**c**) vertical velocity components, (**d**) temperature collected at the highest level (10 m) in the night between the 5 and 6 January 1994

oscillations highlighting a strong correlation of temperature with both kinds of submeso motions. Furthermore, a stronger intermittent energy is observed at smaller turbulent scales, similar to that observed in the vertical velocity component.

The nature of detected vertical structures was analyzed through the wavelet cross-spectral indicators. The comparison between wavelet cospectra (Fig. 10) and quadspectra (Fig. 11) of w and θ highlights a quasi-linear nature of detected waves, in particular at the highest level, where the quadspectral density is greater than the cospectral density. The detected gravity waves persist for just a few cycles and attenuate closer to the ground, where their disruption produces localized mixing at smaller turbulent scales. As a matter of fact, the intensification of the negative values of the computed turbulent momentum and heat fluxes at the lower levels (not shown) highlights the intermittent increasing of turbulent transport induced by the degradation of the gravity-wave events detected at 10 m. The enhanced turbulent mixing observed at the lowest levels may be explained within the framework of the HOST theory, because the composite nature of the background flow and wave oscillations and resultant flow speed may easily exceed the threshold wind speed closer to the ground (see Fig. 3), and generating turbulent eddies capable of vertically mixing both momentum and heat (Sun et al. 2015a, b).

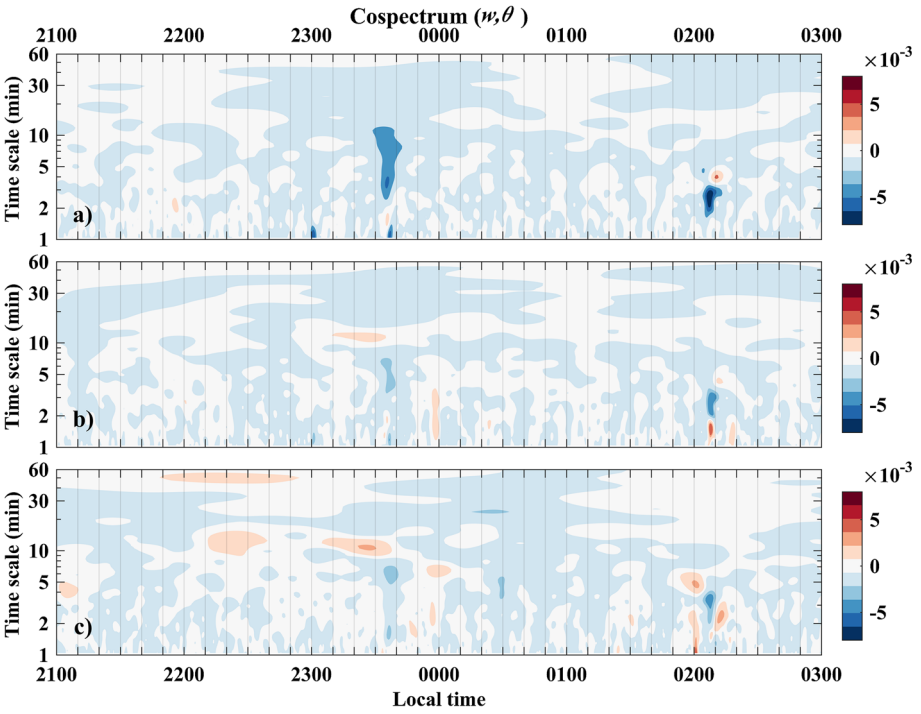

Fig. 10 Time evolution in the submeso time scale range of the wavelet cospectrum for cross-correlation between the vertical velocity component and temperature collected at 10 m (**a**), at 4.5 m (**b**) and at 2 m (**c**) for the night between the 5 and 6 January 1994

3.3.2 Waves Associated with Abrupt and Intermittent Wind-Direction Shifts Modulated by Horizontal Meandering

Figure 12 shows the time series relative to another interesting case study where dirty gravity waves appear periodically superimposed to horizontal meandering and are associated with abrupt and intermittent wind-direction shifts. The selected period is characterized by a mean value of wind speed of ≈ 3 m s^{-1} and by a stability parameter $z/L \approx 3$ at the highest level. Horizontal meandering start after 2100 LT and is characterized by a time scale of about 30–40 min, as highlighted by the wavelet spectra of horizontal components and temperature (Fig. 13a, b, d). The wind direction exhibits a gradual meandering back and forth around a constant mean value throughout the analyzed period; however, abrupt wind-direction jumps (ranging from 30° to 90°) periodically appear as indicated by the arrows in Fig. 12e. In contrast to the most common observed cases such as those described in the previous section, the observed shifts are intermittent and localized in time and do not produce a variation in the mean wind direction, that is they are not related to any change in mean flow dynamics. On the other hand, they are associated with localized sharp decreases in wind speed and temperature and with the appearance of vertical wavelike oscillations superimposed on turbulent fluctuations. The vertical waves have a period of about 4 min (much smaller than for horizontal meandering), as highlighted by the wavelet energy distribution computed at the highest level and shown in Fig. 13. Wavelet cross-spectral analysis highlights that these waves transport momentum, but not heat at the highest level; in fact, the small and sign-oscillating

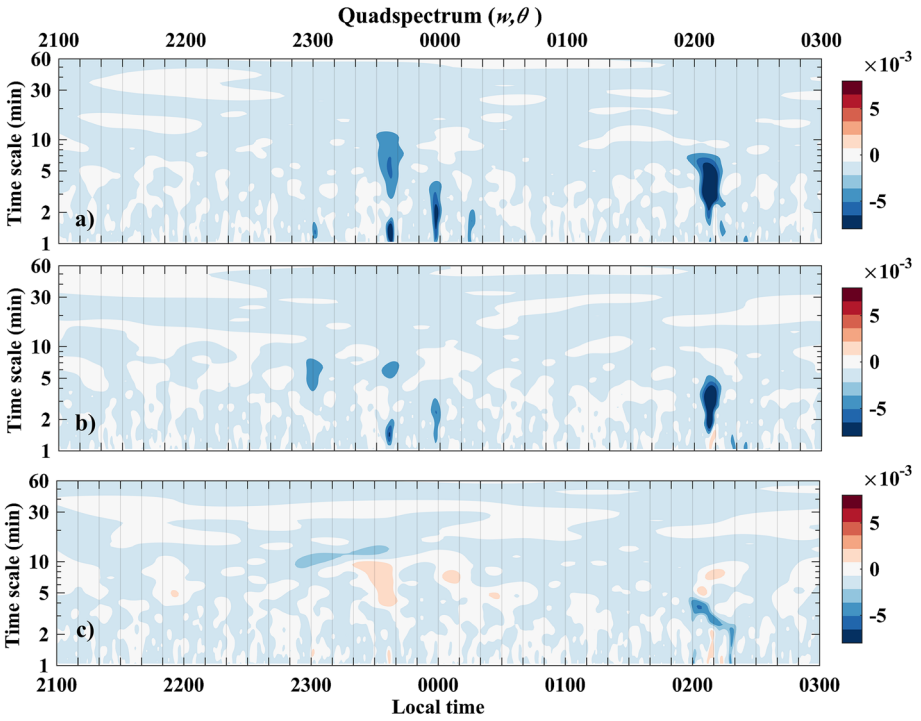

Fig. 11 As for Fig. 10, but for the wavelet quadspectrum for cross-correlation between the vertical velocity component and temperature

wavelet cospectrum ($C_{w\theta}$) and the high value of the quadspectrum ($Q_{w\theta}$) indicate the lack of vertical heat diffusion (i.e. w and θ are 90° out of phase) and the activation of quasi-linear gravity waves (Fig. 14). These waves persist for only a few cycles and tend to be attenuated closer to the surface producing intermittent turbulence, as shown in Fig. 15 for the wavelet cross-spectral analysis for data collected at 4.5 m and in the computed momentum and heat turbulent fluxes (not shown). At this level $Q_{w\theta}$ attenuates and becomes comparable to $C_{w\theta}$ indicating the presence of dirty waves with turbulent fluctuations.

Interestingly, observed intermittent wind-direction shifts appear approximately in correspondence of the crests of the meandering oscillations in the wind direction, that is their period of occurrence is related to the period of horizontal meandering of about 30 min. This fact suggests a possible correlation between observed gravity waves and dynamical instabilities (i.e. shear or thermal instabilities) modulated by horizontal meandering.

4 Summary and Conclusions

The main goal of our study was to investigate the coexistence and interaction of horizontal meandering and gravity waves in the SBL, rarely explored previously. The subject is of relevance because, among different submeso motions, gravity waves and horizontal meandering may play an important role in influencing the flow dynamics and the pollutant dispersion in low-wind-speed and strongly stable conditions.

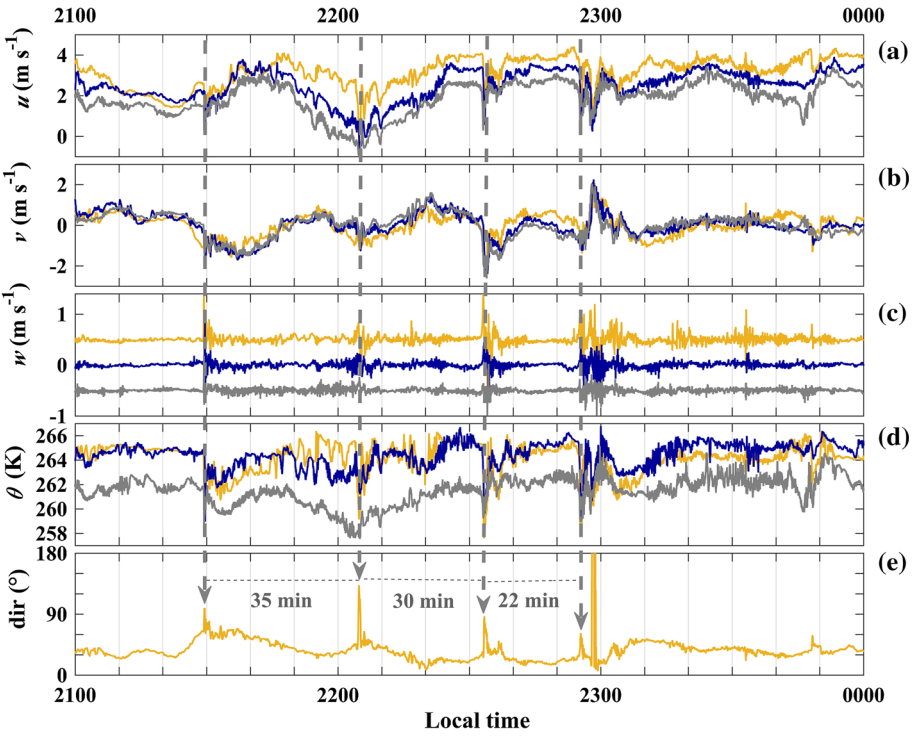

Fig. 12 Time series of longitudinal (**a**), lateral (**b**), vertical velocity components (**c**), temperature (**d**) and wind direction (**e**) collected at different measurement levels (yellow: 10 m, blue: 4.5 m, grey: 2 m) on the 25 November 1993. For a better comparison the time series of w has been artificially shifted (+ 0.5 m s^{-1} at 10 m and − 0.5 m s^{-1} at 2 m) in panel (**c**). Finally, for the sake of clarity the wind direction has been shown only at the highest level in panel (**e**). The arrows in panel (**e**) indicate abrupt and localized wind-direction changes

High-frequency measurements of wind velocity and temperature collected at three levels above an Antarctic Ice Sheet during an austral summer were used, in ideal persistent conditions of strong ABL stratification. The application of two complementary methodologies (the Eulerian-autocorrelation-function technique and the wavelet analysis) allowed the detection and investigation of the nature of submeso motions, their interaction and their influence on an intermittent turbulent field. Meandering activity of the horizontal velocity components was detected at all measurement levels, mainly during nocturnal hours, in strong stability conditions. Horizontal oscillations were frequently associated (in about 50% of the cases) with temperature oscillations characterized by similar meandering time scales ($T_* \approx$ 20–30 min) that remain nearly unchanged at the different measurement heights. On the other hand, vertical oscillations, characterized by T_* of a few minutes, were detected only at the highest level. The attenuation and/or disruption of vertical waves close to the ground may be explained in the framework of the Hockey-stick transition (HOST) theory proposed by Sun et al. (2012, 2015b). As a matter of fact, at the highest measurement level the observed wind-speed threshold between different turbulent regimes was higher than the typical wind speed associated with the detected meandering events. On the other hand, at the lowest heights the wind speed

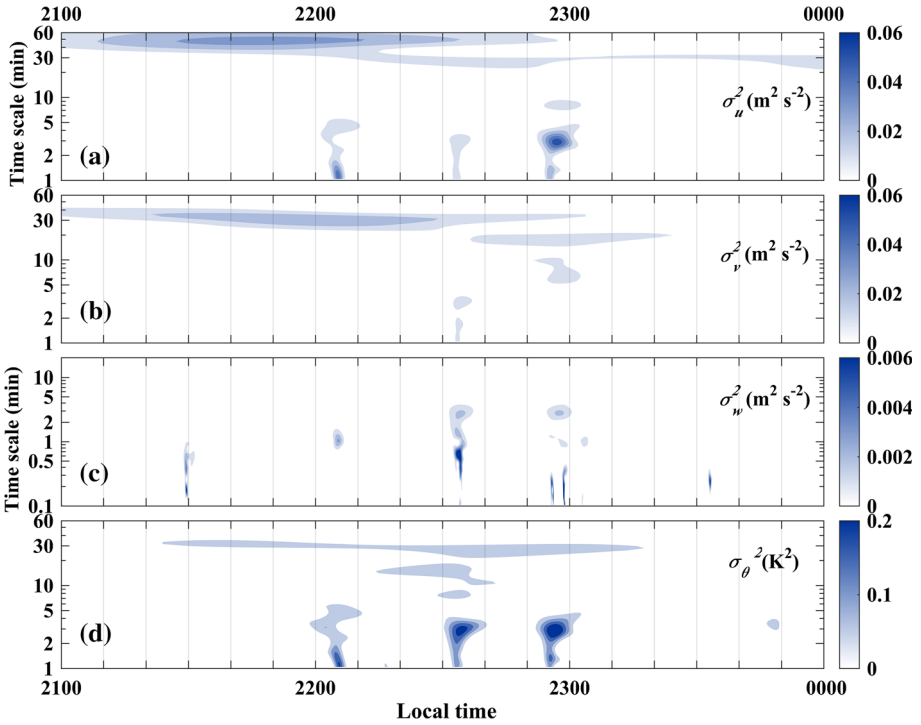

Fig. 13 Time evolution in the submeso time-scale (TS) range of wavelet energy spectra of (**a**) longitudinal, (**b**) lateral and (**c**) vertical velocity components, (**d**) temperature collected at the highest level (10 m) on the 25 November 1993

can readily exceed the corresponding threshold values and the influence of resulting turbulent mixing on gravity waves increases, producing less distinct vertical submeso oscillations near the surface (Sun et al. 2015b).

The meandering imprint was evident also in the spectral behaviour of velocity components and temperature that in the detected cases followed the Kolmogorov (1941) energy decay in the inertial subrange, but deviated from the typical turbulence spectrum at large scales, and exhibited a clear and energetic peak in the low-frequency range. The empirical-averaged spectra were well fitted throughout all the resolved frequencies by the spectral relations proposed by Mortarini and Anfossi (2015) and Mortarini et al. (2016a) for modelling the spectral energy distribution of horizontal velocity components and temperature in low-wind-speed conditions and in the presence of horizontal meandering. Surprisingly, the formula was also successfully applied for fitting the spectral shape in the observed gravity waves, confirming the robustness of the low-wind-speed spectral model.

The performed analysis highlighted the occurrence of frequent large and abrupt wind-direction changes superimposed on the gradual wind meandering, according to other experimental observations (Mahrt 2007, 2008, 2011b; Lang et al. 2018). The fraction of time exhibiting large and abrupt wind-direction shifts ($>\pm 20°$) was about 9% for each hour where submeso motions were detected. This significant occurrence suggests the importance

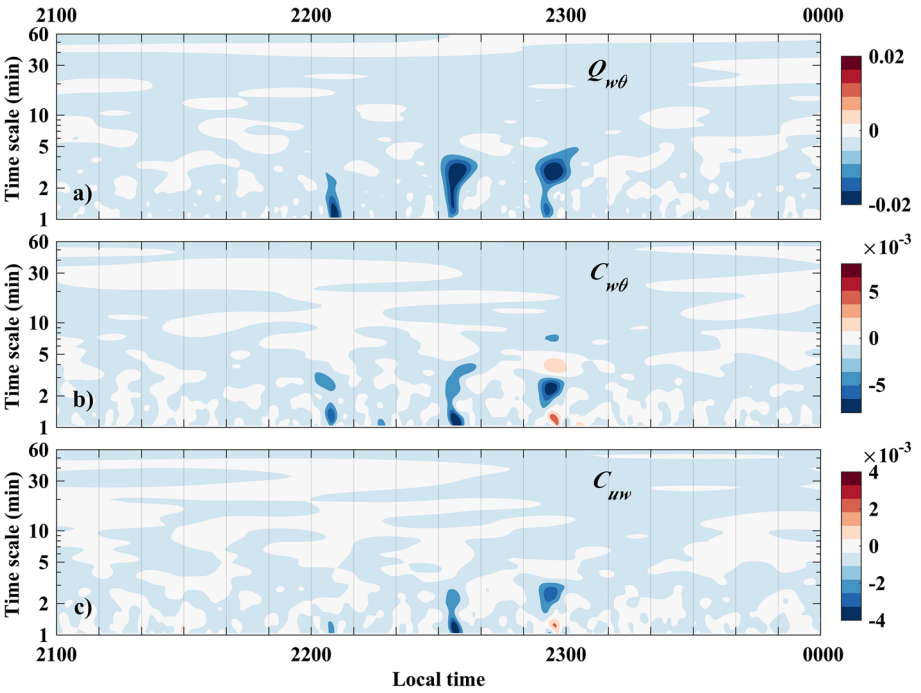

Fig. 14 Time evolution in the submeso time-scale (TS) range of wavelet quadrature (**a**), and cospectrum (**b**) for cross-correlation between vertical velocity component and temperature; and wavelet cospectrum (**c**) for cross-correlation between longitudinal and vertical velocity components collected at the highest level (10 m) on the 25 November 1993

of the wind-direction variability in the flow dynamics of the low-wind-speed SBL. As a matter of fact, the observed gravity waves coexisting with horizontal meandering appeared mostly associated with sharp variations in the mean wind direction related to sudden changes of the mean flow dynamics.

However, other interesting cases displayed gravity waves associated with abrupt and intermittent wind-direction shifts, localized in time and that did not produce any variation in the mean value of the wind direction. It is noteworthy that the intermittent direction shifts, associated with sharp falls of wind speed and temperature, appeared approximately in correspondence of the crests of the meandering oscillations in the wind direction and their period of occurrence seemed related to the horizontal meandering period. This fact may suggest a possible correlation between observed gravity waves and dynamical instabilities (i.e. shear or thermal instabilities) generated by horizontal meandering, that it would be advisable to confirm in future experimental studies.

In all the observed wavy events cross-spectral wavelet analysis indicates that the triggered dirty gravity waves superimposed on horizontal meandering persist for only a few cycles and produce bursts of turbulent mixing close to the ground. The results obtained in this phenomenological study confirm the importance of sharp wind-direction changes in influencing the complex interaction between submeso motions in the SBL. Improved understanding of all the involved processes represents a challenge in the formulation of appropriate parametriza-

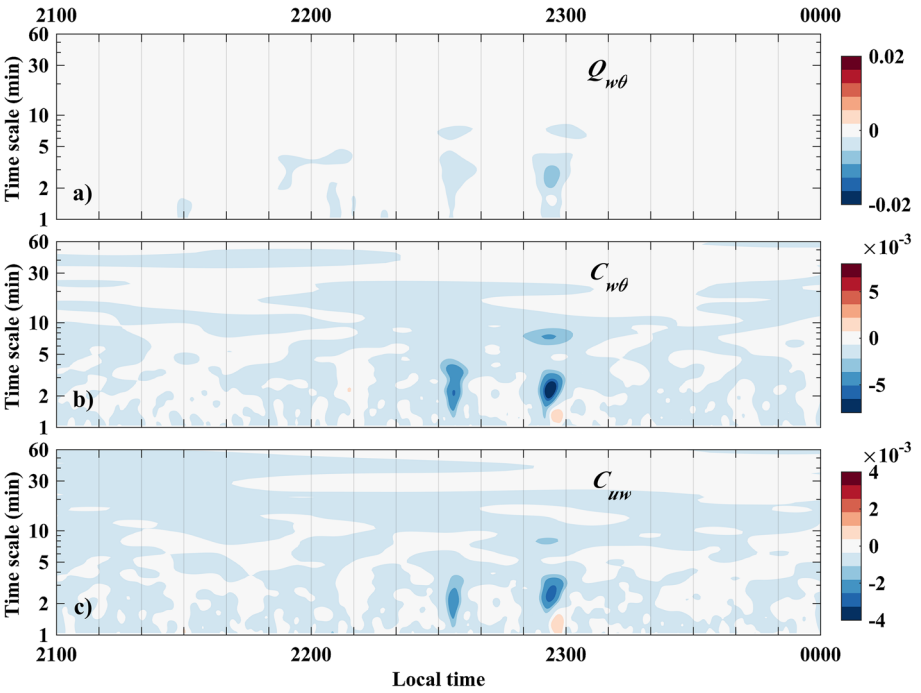

Fig. 15 As for Fig. 14, but for data collected at 4.5 m collected on the 25 November 1993

tions and simulations of horizontal and vertical dispersion at low wind speeds and in very stable conditions.

Acknowledgements This work was supported by PNRA (Progetto Nazionale di Ricerche in Antartide). We would like to acknowledge the collaboration with the Marche Region, and in particular the "Environmental assessments and authorizations, air quality and natural protection" section. We thank Dr. Karl Lapo and the three anonymous reviewers for their constructive comments that contributed to improve the quality of this manuscript.

Appendix 1: Spectral Model for Meandering Motions in Stable and Low-Wind-Speed Conditions

To evaluate the theoretical form of the spectrum in (3), the derivation of Mortarini and Anfossi (2015) has been followed. The normalized Eulerian spectrum, $F_{LW}(n)$, in which t is the time lag and n is the frequency, is (Pasquill 1974; Kaimal and Finnigan 1994)

$$F_{LW}(n) = \frac{S(n)}{\sigma^2} = 4\int_0^\infty R(t)\cos(2\,\pi\, nt)dt \tag{4}$$

Hence, the function

$$F_{LW}(n) = 2p\left[1/\left(p^2 + (q + 2\,\pi\, n)^2\right) + 1/\left(p^2 + (q - 2\,\pi\, n)^2\right)\right] \tag{5}$$

is the spectrum that corresponds to an oscillating autocorrelation function of the form

$$R(t) = \exp(-pt)\cos(qt), \tag{6}$$

where p and q are related to the turbulence decorrelation time scale and to the meandering time scale, respectively. In non-dimensional form, $nF_{LW}(n)$, Eq. 5 presents a distinct maximum

$$[nF_{LW}(n)]_{max} = \left(p^2 + q^2\right)^{\frac{1}{2}}/(\pi\, p) \tag{7}$$

at the frequency

$$n_{max} = \left(p^2 + q^2\right)^{\frac{1}{2}}/(2\pi). \tag{8}$$

It is easily seen that the slope of the asymptotic behaviour in Eq. 5 is -2 and not the prescribed $-5/3$. Equation 5 correctly describes the behaviour of the low-wind-speed spectra close to its maximum value, but it does not take into account the behaviour of the turbulent velocity fluctuations in the inertial subrange. In order to find a spectral form that describes both the low-wind-speed and the Kolmogorov $-2/3$ trends, Mortarini and Anfossi (2015) proposed a linear combination of Eq. 5 with the Kaimal and Finnigan (1994) model for stable conditions,

$$nF_{HW}(n) = A(n/n_0)/\left(1 + A(n/n_0)^{5/3}\right), \tag{9}$$

where n_0 is the frequency at which the extrapolated inertial subrange meets the $nF_{HW}(n) = 1$ line and where $A = 0.164$ for both the three velocity components and the temperature. The meandering spectrum assumes the form

$$F(n, p, q) = \alpha F_{LW}(n, p, q) + \beta(n) F_{HW}(n), \tag{10}$$

where β is heuristically defined as

$$\beta(\tilde{n}) = \left(1 - 2\tilde{n} + \tilde{n}^2\right)/\left(1 + \lambda\tilde{n} + \tilde{n}^2\right), \tag{11}$$

where $\tilde{n} = n/n_{max}$ and λ is a shape parameter that takes into account the energy associated with the intermediate frequency range (i.e. between high and low frequencies), equalling 20 in stable conditions (Mortarini and Anfossi 2015). The parameter α in Eq. 10 is chosen to satisfy the normalization constraint

$$\int_0^\infty F(n, p, q) = 1, \tag{12}$$

i.e.

$$\alpha = 1 - \int_0^\infty \beta(n) F_{HW}(n) dn \tag{13}$$

where the integral is numerically solved using the adaptive quadrature method for each considered time series.

Finally, Eq. 10 can be written as

$$\begin{aligned} F(n, p, q) = 2p\left[\frac{1}{p^2 + (q + 2\,\pi\, n)^2} + \frac{1}{p^2 + (q - 2\,\pi\, n)^2}\right] \\ + \frac{\left(1 - 2\frac{n}{n_{max}} + \left(\frac{n}{n_{max}}\right)^2\right)}{\left(1 + 20\frac{n}{n_{max}} + \left(\frac{n}{n_{max}}\right)^2\right)} \frac{0.0164\frac{n}{n_0}}{1 + 0.0164\left(\frac{n}{n_0}\right)^{5/3}} \end{aligned} \tag{14}$$

which represents the spectra of the velocity components and of the temperature in the presence of submeso wavy motions.

After some algebra (for details, see Mortarini and Anfossi 2015), Eq. 14 can be normalized with the maximum of the low-frequency part of the spectrum (Eq. 7) to obtain,

$$\tilde{F}(\tilde{n}, m) = \frac{\tilde{n}F(\tilde{n}, p, q)}{[nF_{LW}(n)]_{max}} = \alpha \frac{2\tilde{n}\left(1+\tilde{n}^2\right)}{m^2\left(1-\tilde{n}^2\right)^2 + \left(1+\tilde{n}^2\right)^2} + \frac{1-2\tilde{n}+\tilde{n}^2}{1+20\tilde{n}+\tilde{n}^2} \frac{0.515\frac{\tilde{n}}{\gamma}}{\sqrt{m^2+1}\left[1+0.0164\left(\frac{\tilde{n}}{\gamma}\right)^{5/3}\right]}, \tag{15}$$

where $\gamma = (n_0/n_{max})$. The spectral quantity $\tilde{F}(\tilde{n}, m)$ is useful in comparing averaged spectra and it does not depend on p and q separately but only on the ratio m.

The proposed model has been successfully tested for cases corresponding in an oscillatory behaviour in temperature field associated with horizontal meandering (Mortarini et al. 2016a).

Appendix 2: Wavelet Analysis and Cross-Spectral Indicators of Linear Gravity Waves

Wavelet analysis is a useful technique for investigating the intermittent and non-stationary structure of turbulence and its interaction with submeso motions in the ABL (Howell and Mahrt 1997; Cava et al. 2005, 2015, 2017; Viana et al. 2010; Durden et al. 2013; Sun et al. 2015b; Mortarini et al. 2018). The wavelet transform $Wf(\lambda, t)$ of a function $f(t)$ with finite energy is defined as

$$Wf(\lambda, t) = \int_{-\infty}^{\infty} f(u)\psi_{(\lambda,t)}(u)du, \tag{16}$$

where $\psi_{\lambda,t}(u) = \left(1/\lambda^{1/2}\right)\psi((u-t)/\lambda)$ is a family of functions depending on two parameters, a scale parameter $\lambda(>0)$ and a location parameter t. Changing the value of λ has the effect of dilating or contracting the function ψ (called the mother wavelet), i.e. of analyzing the function $f(t)$ at different spatial scales, whereas changing t has the effect of analyzing the function $f(t)$ around the point t.

The wavelet spectrum

$$S = |Wf(\lambda, t)|^2 \tag{17}$$

gives information on the time evolution of the energy of the analyzed signal as a function of the resolved time scales (or frequencies). The wavelet cross-spectrum

$$W_{fg} = Wf(\lambda, t).*Wg(\lambda, t) \tag{18}$$

allows the investigation of the common variability in frequency and time of two different signals (f, g); the cospectrum (C), i.e. the real part of W_{fg}, is proportional to the covariance between the two time series, whereas the quadspectrum (Q), i.e. the complex part of W_{fg}, represents the spectrum of the product of f and g shifted by 90° (Grinsted et al. 2004).

Cross-spectral statistics are very useful in diagnosing the linear nature of vertical wavy events detected in the measured series. In fact, in presence of linear waves, the lack of vertical diffusion produces fluctuations in vertical velocity and scalars 90° out of phase and, as a consequence, the quadspectral density is larger than the cospectral density in the wave source region (de Baas and Driedonks 1985).

For detailed discussions on wavelet theory and applications to the analysis of geophysical data, see Kumar and Foufoula-Georgiou (1997) and Torrence and Compo (1998).

References

Acevedo O, Costa F, Oliveira PES, Puhales FS, Degrazia GA, Roberti DR (2014) The influence of submeso processes on stable boundary layer similarity relationships. J Atmos Sci 71:2017–2225. https://doi.org/10.1175/JAS-D-13-0131.1

Anfossi D, Oettl D, Degrazia G, Goulart A (2005) An analysis of sonic anemometer observations in low wind speed conditions. Boundary-Layer Meteorol 114:179–203. https://doi.org/10.1007/s10546-004-1984-4

Anfossi D, Alessandrini S, Trini Castelli S, Ferrero E, Oettl D, Degrazia G (2006) Tracer dispersion simulation in low wind speed conditions with a new 2D Langevin equation system. Atmos Environ 40:7234–7245. https://doi.org/10.1016/j.atmosenv.2006.05.081

Bates DM, Chambers JM (1992) Nonlinear models. In: Chambers JM, Hastie TJ (eds) Chapter 10 of statistical models in *S*. Wadsworth & Brooks/Cole, Berlin

Belušic D, Güttler I (2010) Can mesoscale models reproduce meandering motions? Q J R Meteorol Soc 136:553–565. https://doi.org/10.1002/qj.606

Cava D, Schipa S, Giostra U (2005) Investigation of low-frequency perturbations induced by a steep obstacle. Boundary-Layer Meteorol 115:27–45. https://doi.org/10.1007/s10546-004-2123-y

Cava D, Giostra U, Katul G (2015) Characteristics of gravity waves over an antarctic ice sheet during an Austral summer. Atmosphere 6:1271–1289. https://doi.org/10.3390/atmos6091271

Cava D, Mortarini L, Giostra U, Richiardone R, Anfossi D (2017) A wavelet analysis of low-wind-speed submeso motions in a nocturnal boundary layer. Q J R Meteorol Soc 143:661–669. https://doi.org/10.1002/qj.2954

de Baas AF, Driedonks GM (1985) internal gravity waves in a stably stratified boundary layer. Boundary-Layer Meteorol 31:303–323. https://doi.org/10.1007/BF00120898

Durden DJ, Nappo CJ, Leclerc MY, Duarte HF, Zhang G, Parker MJ, Kurzeja RJ (2013) On the impact of wavelike disturbances on turbulent fluxes and turbulence statistics in nightime conditions: a case study. Biogeosciences 10:8433–8443. https://doi.org/10.5194/bg-10-8433-2013

Grinsted A, Moore JC, Jevrejeva S (2004) Applications of the cross wavelet transform and wavelet coherence to geophysical time series. Nonlinear Process Geophys 11:561–566. https://doi.org/10.5194/npg-11-561-2004

Güttler I, Belušic D (2012) The nature of small-scale non-turbulent variability in a mesoscale model. Atmos Sci Lett 13:169–173. https://doi.org/10.1002/asl.382

Howell FJ, Mahrt L (1997) Multiresolution flux decomposition. Boundary-Layer Meteorol 83:117–137. https://doi.org/10.1023/A:1000210427798

Kaimal JC, Finnigan JJ (1994) Atmospheric boundary layer flows. Oxford University Press, New York, p 289

Kolmogorov AN (1941) The local structure of turbulence in incompressible viscous fluid for very large Reynolds number. Dokl. Akad. Nauk. SSSR 30:9–13

Kumar P, Foufoula-Georgiou E (1997) Wavelet analysis for geophysical applications. Rev Geophys 35(4):385–412. https://doi.org/10.1029/97RG00427

Lang F, Belušic D, Siems S (2018) Observations of wind-direction variability in the nocturnal boundary layer. Boundary-Layer Meteorol 166:51–68. https://doi.org/10.1007/s10546-017-0296-4

Mahrt L (2007) Weak-wind mesoscale meandering in the nocturnal boundary layer. Environ Fluid Mech 7:331–347. https://doi.org/10.1007/s10652-007-9024-9

Mahrt L (2008) Mesoscale wind direction shifts in the stable boundary-layer. Tellus 60A:700–705. https://doi.org/10.1111/j.1600-0870.2008.00324.x

Mahrt L (2011a) The near-calm stable boundary layer. Boundary-Layer Meteorol 140:343–360. https://doi.org/10.1007/s10546-011-9616-2

Mahrt L (2011b) Surface wind direction variability. J Appl Meteorol Clim 50:144–152. https://doi.org/10.1175/2010JAMC2560.1

Mahrt L (2014) Stably stratified atmospheric boundary layers. Annu Rev Fluid Mech 46:23–45. https://doi.org/10.1146/annurev-fluid-010313-141354

Mahrt L, Mills R (2009) Horizontal diffusion by submeso motions in the stable boundary layer. Environ Fluid Mech 9:443–456. https://doi.org/10.1007/s10652-009-9126-7

Mahrt L, Richardson S, Seaman N, Stauffer D (2012) Turbulence in the nocturnal boundary layer with light and variable winds. Q J R Meteorol Soc 138:1430–1439. https://doi.org/10.1002/qj.1884

Mortarini L, Anfossi D (2015) Proposal of an empirical velocity spectrum formula in low-wind speed conditions. Q J R Meteorol Soc 141:85–97. https://doi.org/10.1002/qj.2336

Mortarini L, Maldaner S, Moor L, Stefanello M, Acevedo O, Degrazia G, Anfossi D (2016a) Temperature autocorrelation and spectra functions in low-wind meandering conditions. Q J R Meteorol Soc 142:1881–1889. https://doi.org/10.1002/qj.2796

Mortarini L, Stefanello M, Degrazia G, Roberti D, Trini Castelli S, Anfossi D (2016b) Characterization of wind meandering in low-wind-speed conditions. Boundary-Layer Meteorol 161:165–182. https://doi.org/10.1007/s10546-016-0165-6

Mortarini L, Cava D, Giostra U, Acevedo O, Nogueira Martins LG, Soares de Oliveira PE, Anfossi D (2018) Observations of submeso motions and intermittent turbulent mixing across a low level jet with a 132-m tower. Q J R Meteorol Soc 144:172–183. https://doi.org/10.1002/qj.3192

Nappo CJ (2002) An introduction to atmospheric gravity waves. Academic Press, New York

Nappo CJ, Sun J, Mahrt L, Belušić D (2014) Determining wave–turbulence interactions in the stable boundary layer. Bull Am Meteorol Soc 95:ES11–ES13. https://doi.org/10.1175/bams-d-12-00235.1

Pasquill F (1974) Atmospheric diffusion. Wiley, London, p 429

R Core Team (2017) R: a language and environment for statistical computing. R Foundation for Statistical Computing, Vienna. https://www.R-project.org/

Sun J, Mahrt L, Banta RM, Pichugina YL (2012) Turbulence regimes and turbulence intermittency in the stable boundary layer during CASES-99. J Atmos Sci 69:338–351. https://doi.org/10.1175/JAS-D-11-082.1

Sun J, Nappo CJ, Mahrt L, Belušic D, Grisogono B, Stauffer DR, Pulido M, Staquet C, Jiang O, Pouquet A, Yagüe C, Galperin B, Smith RB, Finnigan JJ, Mayor SD, Svensson G, Grachev AA, Neff WD (2015a) Review of wave-turbulence interactions in the stable atmospheric boundary layer. Rev Geophys 53:956–993. https://doi.org/10.1002/2015RG000487

Sun J, Mahrt L, Nappo C, Lenschow DH (2015b) Wind and temperature oscillations generated by wave–turbulence interactions in the stably stratified boundary layer. J Atmos Sci 72:1484–1503. https://doi.org/10.1175/JAS-D-14-0129.1

Thomas C, Foken T (2005) Detection of long- term coherent exchange over spruce forest using wavelet analysis. Theor Appl Climatol 80:91–104. https://doi.org/10.1007/s00704-004-0093-0

Torrence C, Compo GP (1998) A practical guide to wavelet analysis. Bull Am Meteorol Soc 79:61–78. https://doi.org/10.1175/1520-0477(1998)079%3c0061:APGTWA%3e2.0.CO;2

Viana S, Terradellas S, Yague C (2010) Analysis of gravity waves generated at the top of a drainage flow. J Atmos Sci 67:3949–3966. https://doi.org/10.1175/2010JAS3508.1

Vickers D, Mahrt L (2006) A solution for flux contamination by mesoscale motions with very weak turbulence. Boundary-Layer Meteorol 118:431–447. https://doi.org/10.1007/s10546-005-9003-y